ACS APPLIED MATERIALS & INTERFACES

Research Article

www.acsami.org

Enhanced Electroresponse of Alkaline Earth Metal-Doped Silica/Titania Spheres by Synergetic Effect of Dispersion Stability and Dielectric Property

Chang-Min Yoon, Seungae Lee, Oug Jae Cheong, and Jyongsik Jang*

School of Chemical and Biological Engineering, Seoul National University, 599 Gwanak-ro, Gwanak-gu, Seoul 151-742, Korea

Supporting Information

ABSTRACT: A series of alkaline earth metal-doped hollow SiO_2/TiO_2 spheres (EM-HST) are prepared as electrorheological (ER) materials via sonication-mediated etching method with various alkaline earth metal hydroxides as the etchant. The EM-HST spheres are assessed to determine how their hollow interior and metal-doping affects the ER activity. Both the dispersion stability and the dielectric properties of these materials are greatly enhanced by the proposed one-step etching method, which results in significant enhancement of ER activity. These improvements are attributed to increased particle mobility and interfacial polarization originating from the hollow nature of the EM-HST spheres and the effects of EM metal-doping. In particular, Ca-HST-based ER fluid exhibits ER performance which is 7.1-fold and 3.1-fold higher than those of nonhollow core/shell silica/titania (CS/ST) and undoped hollow silica/titania (HST)-based ER fluids, respectively. This study develops a versatile and simple approach to enhancing ER activity through synergetic effects arising from the combination of dispersion stability and the unique dielectric properties of hollow EM-HST spheres. In addition, the multigram scale production described in this experiment can be an excellent advantage for practical and commercial ER application.

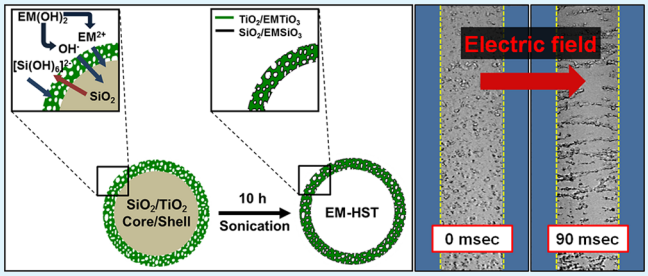

KEYWORDS: *alkaline earth metal, hollow, metal-doping, electroresponsive, electrorheology, silica, titania*

INTRODUCTION

Electrorheological (ER) fluids are suspensions composed of polarizable particles dispersed in an insulating medium. Such materials can form fibril-like structures under an applied external electric field. ER fluids have been studied extensively due to their tunability, simple mechanism, reversibility, fast response, and low power consumption.[1−3] Due to their versatility, ER fluids are often applied as materials in clutches, dampers, and haptic devices.[4,5] A variety of polarizable metallic, polymeric, and inorganic particles have been adopted as ER materials.[6−10] Previous researchers have attempted to increase the ER activity by controlling the properties of materials. In particular, ER activity can be greatly enhanced by altering the dispersion stability and dielectric properties of the particles.

Dispersion stability, or the antisedimentation properties of a material, is regarded as one of the most important factors affecting ER efficiency. Materials with a low dispersion stability exhibit relatively low ER activity because of sedimentation, which prevents the formation of fibril-like structures when an electric field is applied.[11,12] Thus, high dispersion stability is essential to maximize ER performance. The dispersion stability of ER materials has been enhanced by controlling the pore size, density, and mass of the dispersed particles. For example, Yoon et al. synthesized mesoporous silica spheres with enhanced ER performance by simultaneously decreasing both the particle density and mass.[13] Lee et al. enhanced the dispersion stability of ER fluids by controlling the size of the silica spheres.[14]

ER efficiency is also affected by the polarizability of the material. In general, the polarizability of a material is determined by its dielectric properties and related parameters.[15] The dielectric properties of a given material can be improved by increasing the polarizable area, creating a composite material, or by metal-doping.[16−18] Recently, due to its relative simplicity, doping with alkaline earth metals has been widely used to increase the dielectric properties of ER materials. For example, Kim et al. successfully doped barium into a silica/titania composite to enhance both the dielectric properties of the material and its ER activity.[19] However, it is important to select an appropriate material and doping level in order to avoid electrical shorts.[7] In other words, an applicable conductivity range must be maintained.

Recently, hollow-structured materials have received considerable attention as suitable candidates for ER materials because of their high active surface area and outstanding dispersion stability. Compared to nonhollow (or packed) particles, these hollow structures combine the advantage of dispersibility with low particle mass and density.[20,21] The surface of the inner

Received: March 18, 2015
Accepted: August 12, 2015
Published: August 12, 2015

DOI: 10.1021/acsami.5b02388
ACS Appl. Mater. Interfaces 2015, 7, 18977−18984

cavity also provides more polarizable area.[22] Among the various hollow-structured materials that have been developed, the most widely studied are silica (SiO_2) and titania (TiO_2) because of their facile synthesis and availability for mass production. Many studies have reported the synthesis of hollow particles of silica and titania. For example, Chen et al. synthesized porous hollow silica materials using a calcium carbonate template.[23] Choi et al. reported the fabrication of gram-scale silica/titania hollow composites via an etching process using ammonium hydroxide.[24] However, silica has naturally low ER activity because of its inherently low electrical conductivity.[25] For practical applications, the dielectric properties of such material must be enhanced. On the other hand, titania can be a good candidate for ER materials owing to its outstanding dielectric property.[26] Many kinds of titania and its derived forms were adopted as ER materials including polymer-coated titania, shape-modified titania, crystalline titania, and rare-earth-doped titania.[27−30] Moreover, silica and titania composite materials are also studied for their combined ER activity.[31,32]

Herein, we describe the fabrication of alkaline earth metal-doped hollow silica/titania spheres (EM-HST) using a facile synthesis method. The resulting particles exhibit synergetic effects because of the combination of their enhanced dispersion stability and dielectric properties. To the best of our knowledge, this is the first experiment to explore how the series of alkaline earth metal-doping (Ba, Sr, and Ca) affects ER activity of silica/titania hollow composites. Gram-scale quantities of porous core/shell silica/titania (CS/ST) spheres were easily fabricated using a sol−gel method. Subsequently, porous CS/ST spheres were etched by alkaline earth metal hydroxides using a sonication-mediated etching and redeposition (SMER) method to obtain EM-HST spheres. This simple etching method enabled both metal-doping and fabrication of hollow materials in a single step. The resulting EM-HST spheres exhibited dramatic increases in their dielectric properties and dispersion stability, and also exhibited excellent ER performance in practical applications.

MATERIALS AND METHODS

Materials. Tetraethyl orthosilicate (TEOS), titanium isopropoxide (TTIP, 97.0%), barium hydroxide, calcium hydroxide, magnesium hydroxide, strontium hydroxide, and silicone oil [poly(methylphenylsiloxane), viscosity = 100 cSt, dielectric constant = 2.73, electrical conductivity = 1×10^{-13} S m^{-1}][33] were purchased from Aldrich Chemical Co. Absolute ethanol (ethyl alcohol, 99.5%) was purchased from Fisher Chemical Co. Ammonium hydroxide (NH_4OH, 28.0−30.0%) and acetonitrile (CH_3CN, 99.8%) were purchased from Samchun Chemical Co. (Korea). All of chemicals were used without further purification.

Synthesis of Porous Core/Shell SiO_2/TiO_2 (CS/ST Spheres). A silica (SiO_2) colloidal suspension was fabricated according to the Stöber method. Titania (TiO_2) shells were coated onto the core SiO_2 spheres via sol−gel reaction. A mixture of titanium isopropoxide (6 mL), absolute ethanol (36 mL), and acetonitrile (12 mL) was slowly added to the as-synthesized SiO_2 colloidal solution. The resulting colloidal suspension was stirred at 4 °C for 12 h to obtain porous core/shell SiO_2/TiO_2 spheres (CS/ST spheres). Finally, the porous CS/ST spheres were collected by centrifugation and dried overnight.

Fabrication of Alkaline Earth Metal-Doped Hollow SiO_2/TiO_2 Spheres (EM-HST Spheres). Alkaline earth metal-doped hollow SiO_2/TiO_2 (EM−HST) spheres were synthesized using a modified sonication-mediated etching and redeposition (SMER) method developed by Choi et al.[24] Dried CS/ST spheres (0.5 g) were dispersed in deionized water (12 mL) and sonicated for 3 h. Various alkaline earth metal hydroxides (3.0 mL, 0.1 M of $Ca(OH)_2$, 0.15 M of $Sr(OH)_2$, or 0.2 M of $Ba(OH)_2$) were added to the above solution and sonicated for 12 h. The alkaline earth metal hydroxides were fabricated according to the following two steps. First, solid alkaline earth metal hydroxides were added to DI water and sonicated for 10 h. Second, the resulting mixture was cooled in an ice bath for 3 h to precipitate insoluble metal hydroxide species. Subsequently, only the top part of solution without hydroxide sediments was recovered. The above steps were repeated for several times. The metal-doping and core-etching processes were performed simultaneously by using the alkaline earth metal hydroxide solution as the etchant. The resulting white cloudy solution containing EM-HST spheres was centrifuged several times with deionized water to remove any remaining hydroxide species and dried overnight at 60 °C. All of the EM-HST spheres were fabricated using the same procedure but with different alkaline earth metal hydroxides. The yield of various EM-HST spheres were about ∼0.3 g, by following the above process. Undoped hollow SiO_2/TiO_2 (HST) spheres were also fabricated using this same method with NH_4OH (0.1 M) as the etchant solution. In addition, etching process can be scaled up to 20 times by increasing the amount of CS/ST spheres, deionized water, and amount of various alkaline earth metal hydroxides to obtain maximum of ∼6.0 g of EM-HST spheres.

Characterization. The morphologies of CS/ST, HST, and various EM-HST spheres were characterized by TEM analysis (JEM-200CX, JEOL) and FE−SEM observation (JEOL-6700, JEOL). Pore size and internal cavity volumes were determined by BJH measurements (ASAP-2010, Micrometrics). Atomic weight percentages of O, Si, Ti, Ca, Sr, and Ba were obtained using an FE-SEM (JEOL-6700, JEOL) equipped with an EDS spectrometer (INCA energy). STEM-EDS elemental mapping was provided by STEM (Tecnai F20, FEI) with a Gatan image filter (Gatan, Inc.). XPS spectra were obtained with M18XHF−SRA (MAC Science Co.) and AXIS−His (KRATOS) spectrometers. Dielectric properties were investigated by impedance spectroscopy (Solatron-1260) and a dielectric interface analyzer (Solatron-1296).

Investigation of Electrorheological (ER) Properties. To prepare ER fluids, dried particles (110 °C for 24 h in the oven) were well-dispersed in silicone oil (poly(methylphenylsiloxane), viscosity = 100 cSt) using magnetic stirrer. The concentration of all ER fluids was set to 30 vol %, and no additives were added to the sample. The ER property of prepared samples were examined using sets of rheometer (AR2000 Advanced Rheometer, TA Instruments) with a cup (diameter = 30.0 mm, height = 30.0 mm), a concentric cylinder conical geometry (diameter = 28.0 mm, internal height = 30.0 mm) and a high voltage generator (Trek 677B). The gap distance between the cup and rotor of geomerty was fixed to 1.00 mm. The ER measurements were started by placing ER fluids between the cup and rotor. Subsequently, mechanical shear (1.0 s^{-1}) was applied for 3 min to obtain an equilibrium state. Lastly, DC voltage was applied to investigate ER property of various ER fluids. Also, the real leakage current and current density for ER fluids was measured from the high voltage generator by using 40.0 mm of steel plate geometry instead of concentric cylinder conical.

RESULTS AND DISCUSSION

The schematic procedure for fabrication of alkaline earth metal-doped SiO_2/TiO_2 hollow spheres (EM-HST) is illustrated in Figure 1. First, silica core templates were synthesized using the Stöber method. TTIP precursor was then added dropwise to the SiO_2 colloidal solution to afford porous core/shell SiO_2/TiO_2 (CS/ST) spheres via sol−gel condensation. Finally, the porous CS/ST was etched under sonication with various $EM(OH)_2$ solutions (EM = Ca, Sr, and Ba) to synthesize EM-HST spheres. Undoped hollow silica/titania (HST) spheres were fabricated using a solution of NH_4OH as the etchant. Particularly, the concentration of etchant solutions played as a key role for minimizing the partial etching of SiO_2 core and formation of particle aggregation (see Figure S1). A detailed evolutionary mechanism for etching process of various EM-

DOI: 10.1021/acsami.5b02388
ACS Appl. Mater. Interfaces 2015, 7, 18977−18984

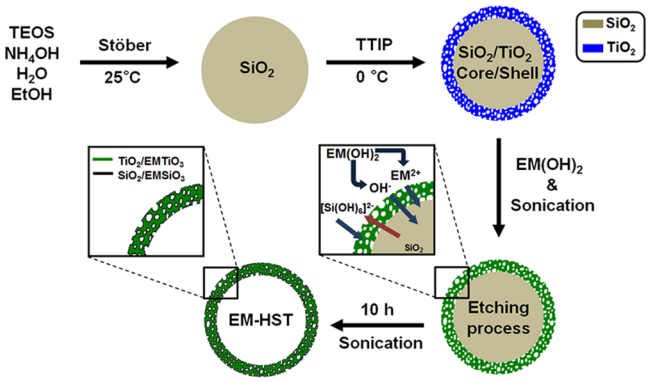

Figure 1. Schematic illustration for the synthesis of various alkaline earth metal-doped hollow silica/titania sphere (EM-HST) via Stöber, sol–gel, and sonication-mediated etching and redeposition (SMER) method.

HST and HST spheres are further described in Figure S2 (see Supporting Information).

Transmission electron microscope (TEM) analysis was carried out to confirm the successful formation of HST and various EM-HST spheres, as shown in Figure 2. The spheres

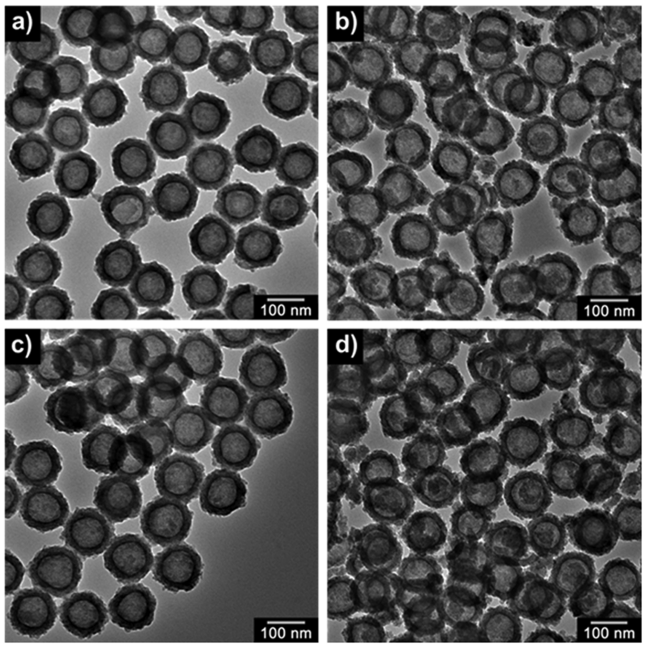

Figure 2. Representative TEM micrograph of (a) HST, (b) Ca-HST, (c) Sr-HST, and (d) Ba-HST. All samples were homogeneously fabricated with hollow interior strucuture and similar diameter of ~130 nm.

were highly uniform with a diameter of ~130 nm. Note that, for all samples, internal hollow spaces were created within the outer shells, indicating successful etching of the SiO_2 core template. The scanning electron microscope (SEM) image of various EM-HST spheres also displayed uniform natures of materials without particle aggregation (see Figure S3). Some of outer shells were broken during the etching process and internal hollow cavity was able to seen by the SEM observation.

To further characterize the internal structure of the spheres, BJH pore distributions and BET surface areas were determined from N_2-sorption isotherms. Figure 3 shows that the HST and EM-HST spheres were synthesized with small intrapores of ~4 nm on the outer shell. The N_2-sorption curves from all of the samples revealed typical type IV hysteresis loops for porous materials (Figure 3, inset). The internal cavities of the HST, Ca-HST, Sr-HST, and Ba-HST spheres measured 75.17, 73.42, 69.46, and 69.42 nm, respectively (see Table S1). Most notably, the volume of the sphere interior decreased with increasing molar mass of the $EM(OH)_2$ etchant solution. This phenomenon was explained by Kim et al.[34] During the etching process, the siloxane bond of SiO_2 is dissolved by the basic solution and recoordinated with OH^- ions to form $[Si(OH)_6]^{2-}$ ions (silicic acid). A detailed mechanism for etching process of hollow silica/titania spheres is described in our previous studies.[24,34] Subsequently, these $[Si(OH)_6]^{2-}$ ions react with EM^{2+} ions and redeposit onto the surface as EM-silicates ($EMSiO_3$). Thus, the Ba-HST spheres contained the smallest internal volume due to the redeposition of Ba-silicate compounds, which are larger than Sr or Ca-silicates. Additionally, Ba-HST had the lowest BET surface area and pore volume, which is consistent with this trend (see Table S2). Conversely, the Ca-HST spheres contained the largest internal volume, the greatest BET surface area, and the largest pore volume.

The elemental composition of each sample was determined by energy-dispersive X-ray spectroscopy (EDS) (see Table S3). Undoped CS/ST and HST spheres were contained only Si, Ti, and O atoms. In addition to these elements, specific EM metals, Ca, Sr, and Ba, were detected in the Ca-HST, Sr-HST, and Ba-HST spheres, respectively. The HST and EM-HST spheres contained less Si than the CS/ST spheres. This phenomenon was caused by etching of the silica core template. Figure 4 gives an elemental map of EM metals on the various EM-HST spheres, obtained by scanning transmission electron microscopy (STEM). Si, Ti, and O atoms were distributed throughout the sphere material. Additionally, each of the Ca, Sr, and Ba metals was successfully doped over the entire surface of the spheres, resulting in hybrid EM-HST spheres.

X-ray photoelectron spectroscopy (XPS) was used to further clarify the molecular structures of the CS/ST, HST, and EM-HST sphere. The Si (2p) spectrum of the CS/ST, HST, and various EM-HST spheres were investigated. Particularly, nonhollow CS/ST spheres were detected with only one peak at 101.8 eV, which is indicating the silica peak (Figure 5a). On the other hand, hollow structured spheres fabricated by redeposition process had two deconvoluted peaks located near 101.8 eV (silica, blue) and 102.5 eV (silicate, red) (Figure 5b–e). The investigation of O (1s) spectrum of samples supported the difference between CS/ST and hollow materials. The CS/ST spheres were deconvoluted into three different peaks of O 1s signals (Figure 5f). However, various EM-HST spheres had additional O 1s signal locating at 531.5 eV, which is attributed from the presence of silicates (Figure 5g–j). Interestingly, small peaks corresponding to titanate (458.3 and 468.3 eV, red) were observed in the XPS spectra of the EM-HST spheres after deconvolution (see Figure S4). While TiO_2 bonding is stronger than that of SiO_2, small amounts of TiO_2 were dissolved to form EM-titanates ($EMTiO_3$) through a process analogous to the formation of silicates. Also, Ca (2p), Sr (3d), and Ba (3d) peaks were evident in the XPS spectra of the EM-HST spheres (see Figure S5). These results show that EM-HST spheres were coated entirely with EM-silicate with small amounts of EM-titanate.

Figure 6 shows the dispersion stability of CS/ST, HST, and EM-HST sphere-based ER fluids in silicone oil (30.0 vol %).

DOI: 10.1021/acsami.5b02388
ACS Appl. Mater. Interfaces 2015, 7, 18977–18984

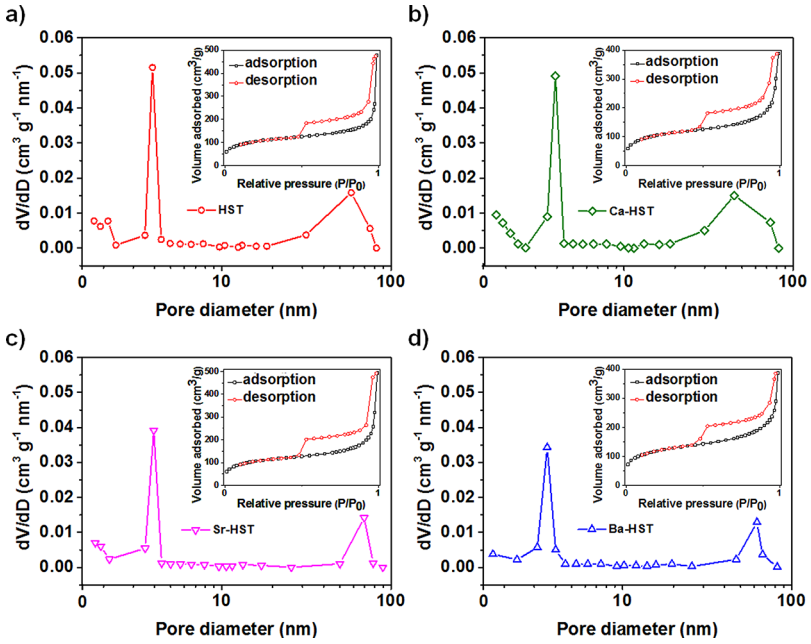

Figure 3. BJH pore distribution curve of (a) HST, (b) Ca-HST, (c) Sr-HST, and (d) Ba-HST [inset: N_2-sorption curve]. Small pores (~4 nm) were created on the surface of outer shell. Also, N_2-sorption curves of all samples exhibited typical Type IV hysteris loop, which indicated the porous natures of material.

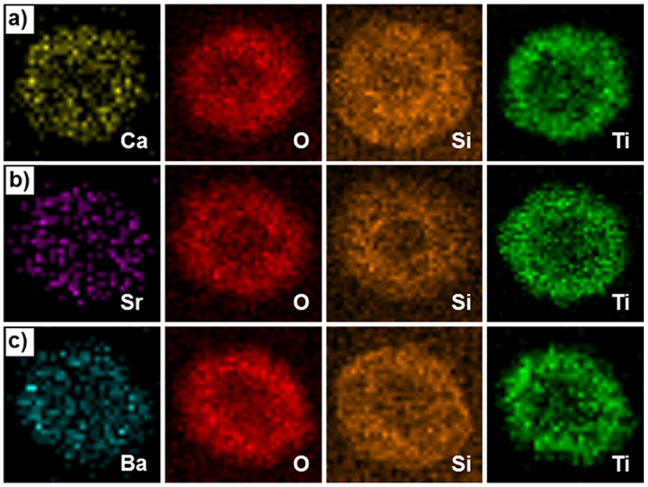

Figure 4. STEM-elemental-mapping analysis of (a) Ca-HST, (b) Sr-HST, and (c) Ba-HST, respectively. Specific alkaline earth metals were successfully doped onto the entire surface of hollow SiO_2/TiO_2 spheres.

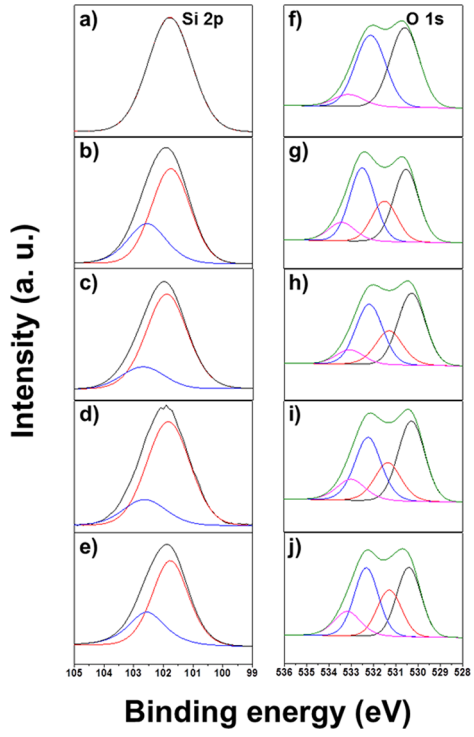

Figure 5. XPS Si 2p level spectra for (a) CS/ST, (b) HST, (c) Ca-HST, (d) Sr-HST, and (e) Ba-HST, respectively (deconvoluted components blue, SiO_2; red, $EMSiO_3$). XPS O 1s level spectra for (f) CS/ST, (g) HST, (h) Ca-HST, (i) Sr-HST, and (j) Ba-HST, respectively.

Well-dispersed samples gradually formed sediments and reached an equilibrium state after 60 h. The nonhollow CS/ST sphere-based ER fluids had the lowest dispersion stability with a sedimentation ratio (R) of 0.8 because of their relatively high particle mass and density. In contrast, the HST and EM-HST sphere-based ER fluids had relatively high sedimentation ratios ($R > 0.85$), indicating their suitability for ER applications by preventing sedimentation and particle aggregation. Moreover, previous studies have shown that particle mobility increases with dispersion stability.[35,36] This enhanced mobility can result in direct improvements to ER activity by allowing the rapid formation of fibril-like structures. Note that the Ca-HST sphere-based ER fluid exhibited excellent sedimentation properties and the highest sedimentation ratio (R = 0.9) of the undoped HST-based ER fluids. Among the hollow sphere materials, the Ba-HST ER fluid had low dispersion stability due to the presence of heavy Ba-silicates. To gain deeper insight into the dispersion stability of various EM-HST spheres, particle density was determined by using a hydrometer at a standard condition. Determined densities for CS/ST, HST, Ca-

DOI: 10.1021/acsami.5b02388
ACS Appl. Mater. Interfaces 2015, 7, 18977−18984

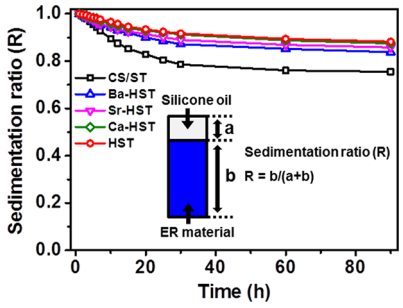

Figure 6. Sedimentation properties of CS/ST, HST, and various EM-HST spheres-based ER fluids dispersed in silicone oil (30.0 vol %). Inset: Illustrated definition of sedimentation ratio.

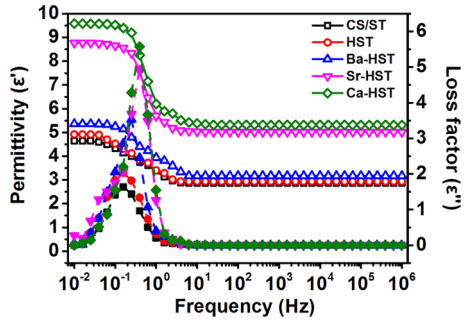

Figure 7. Permittivity (ε', open symbol) and loss factor (ε'', closed symbol) as a function of electric field frequency (f) for CS/ST, HST, and EM-HST-based ER fluids (30.0 vol %) well dispersed in silicone oil.

HST, Sr-HST, and Ba-HST spheres were ~2.74, 2.65, 2.67, 2.69, and 2.72 g cm^{-3}, respectively. The particle density agreed to the trend of sedimentation properties discussed above. The CS/ST spheres showed highest particle density due to the presence of core SiO_2. On the other hand, hollow structured silica/titania spheres were obtained with relatively low particle density. Among the hollow materials, Ba-HST spheres had lowest particle density owing to the formation of Ba-silicates. Additionally, various EM-HST spheres-based ER fluids were further investigated by applying Stokes' relation to determine the theoretical sedimentation velocity. The equation for Stokes' law is described as follows:

$$V_g = d^2(\rho_p - \rho_l)/18\eta \times G$$

Here, V_g is the sedimentation velocity of particle, d is the diameter of particle, p_p is the particle density, p_l is the liquid density, η is the viscosity of liquid, and G represents the gravitational acceleration. The sedimentation velocity of ER fluids were calculated and determined values were 1.71×10^{-10}, 1.62×10^{-10}, 1.64×10^{-10}, 1.66×10^{-10}, and 1.69×10^{-10} m s^{-1} for CS/ST, HST, Ca-HST, Sr-HST, and Ba-HST-based ER fluids, respectively. As a result, HST and Ca-HST spheres with low particle density exhibited relatively slow sedimentation velocity, which implied the enhanced dispersion stability. The physical parameters and sedimentation velocities of various EM-HST spheres-based ER fluids are listed in Table S4 (see Supporting Information). These results show that EM metals were successfully doped onto the surface of SiO_2/TiO_2 composites with minimal losses of dispersion stability.

The dielectric constants (ε') and loss factors (ε'') of the EM-HST sphere-based ER fluids were investigated to determine the effects of dielectric properties on ER activity, as shown in in Figure 7. In general, the dependence of ER performance on dielectric parameters is explained by the achievable polarizability ($\Delta\varepsilon$) and relaxation time (λ).[37,38] The achievable polarizability is defined by the difference between the static permittivity ($f \to \infty$) and the fictitious permittivity ($f \to 0$) of a given material and indicates its tendency for polarization.[39] The relaxation time, which is related to the efficiency of interfacial polarization, can be estimated using the equation[40]

$$\lambda = \frac{1}{2\pi f_{max}}$$

where f_{max} is the maximum frequency of the dielectric loss factor. ER fluids with larger achievable polarizabilities and shorter relaxation times are known to exhibit better ER activities.[15,41] Hollow HST and EM-HST-based ER fluids had higher $\Delta\varepsilon$ and shorter λ values compared with nonhollow CS/ST-based ER fluids (Table 1). Additionally, all of the EM-HST-based ER fluids exhibited improved dielectric properties relative to those of HST-based ER fluids. This may be attributed to the formation of EM-silicates and titanates with high dielectric properties. Among the EM-HST-based ER fluids, the Ca-HST-based ER fluid exhibited the highest $\Delta\varepsilon$ and shortest λ because of the relatively small ionic radius of the Ca dopant. This phenomenon is consistent with the findings of previous studies that correlate dielectric constants with ionic radii of various dopants.[42−44] This outcome also indicates that the EM-HST-based ER fluids had better dielectric properties than the nonhollow CS/ST or undoped HST-based ER fluids, making them more appropriate for ER materials.

Table 1. Dielectric Parameters of CS/ST, HST, and Various EM-HST-Based ER Fluids[a]

	ε_0	ε_∞	$\Delta\varepsilon = (\varepsilon_0 - \varepsilon_\infty)$	f_{max}[b] (Hz)	λ[c] (s)
CS/ST	4.64	2.87	1.77	0.16	0.99
HST	4.92	2.94	1.98	0.16	0.99
Ba-HST	5.36	3.17	2.19	0.25	0.63
Sr-HST	8.77	5.01	3.76	0.39	0.40
Ca-HST	9.58	5.31	4.27	0.39	0.40

[a]Dielectric properties were determined by impedance analyzer (1260, Solatron) coupled with dielectric interface (1296, Solatron). [b]The local frequency of the peak from the dielectric loss factor ε'' and the f_{max} values were measured by nonlinear regression using OriginPro. [c]The relaxation time was measured using $\lambda = 1/(2\pi f_{max})$ relation (f_{max} is the maximum frequency of the loss peak).

Figure 8a shows shear stress curves of CS/ST, HST, and EM-HST-based ER fluids as a function of shear rate (r') under an electric field of 3.0 kV mm^{-1} (30.0 vol % in silicone oil). The real leakage current of CS/ST, HST, Ca-HST, Sr-HST, and Ba-HST-based ER fluids were determined as 0.021, 0.029, 0.043, 0.039, and 0.031 mA, respectively, under 3.0 kV mm^{-1} of electric field. Also, the current density of samples under 3.0 kV mm−1 of electric field was measured as 1.67, 2.31, 3.42, 3.11, and 2.47 μA cm^{-2}, respectively. With the applied external electric field, all of the ER fluids exerted an immediate shear stress due to the creation of chain-like structures by electrostatic forces. The HST and EM-HST-based ER fluids generated higher shear stresses than those of nonhollow CS/ST-based ER fluids. This outcome suggests that the increased dispersion stability of hollow sphere-based materials, and the resulting enhancement in particle mobility, developed as

DOI: 10.1021/acsami.5b02388
ACS Appl. Mater. Interfaces 2015, 7, 18977−18984

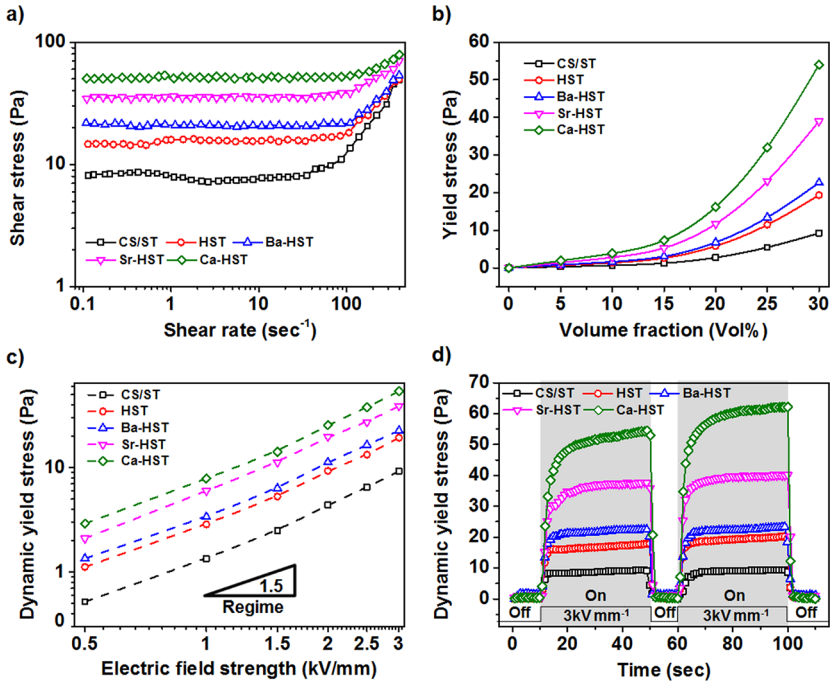

Figure 8. ER activity of CS/ST, HST and various EM-HST-based ER fluids as a function of (a) shear rate (30.0 vol %, 3 kV mm^{-1}), (b) volume fraction, and (c) electric field strength, respectively. (d) Real-time response of ER fluids (30.0 vol %) by on−off test under 3 kV mm^{-1}.

enhanced ER performance. In particular, the Ca-HST-based ER fluids exhibited the highest ER activity, followed by Sr, Ba, and HST-based ER fluids. This trend is consisted with the previously discussed trend in dielectric parameters. Thus, doping HST spheres with EM metals significantly improved the interfacial and particle polarization abilities of the spheres, resulting in higher shear stresses.

In the low shear rate region, all of the ER fluids exhibited typical Bingham plastic behavior consisting of plateau curves that result from competition between interparticle forces and the applied hydrodynamic force.[45] The shear stress of all of the ER fluids increased suddenly in the high shear rate region after passing a critical shear rate (r'_{crit}). Thereafter, Newtonian (or shear thinning) behavior was observed in which the applied hydrodynamic force dominated the electrostatic forces between particles.[46,47] Moreover, the ER activity of all samples at the zero field condition was investigated (see Figure S6). All shear stress curves exhibited Newtonian behavior with increasing shear rate. Interestingly, shear stresses of various EM-HST spheres were similar, but slightly low values for the CS/ST-based ER fluids was investigated. This phenomenon is attributed from the particle density of materials. Due to the high particle density, the dispersion stability of CS/ST-based ER fluids decreased, which also reduced the number of particle−particle interaction by sedimentations.[48] Consequently, nonhollow CS/ST exerted slightly low ER performance at the zero field condition compared to hollow materials. In addition, the cycling temperature test was performed to investigate the temperature effect on the samples (see Figure S7). With an increasing temperature, yield stresses of all sample without an electric field decreased due to the decreasing tendency of zero-field viscosity of silicone oil medium.[48,49] On the other hand, yield stresses of various EM-HST spheres-based ER fluids increased with rising temperature under an electric field of 3.0 kV mm^{-1}. This behavior is related to the dielectric constant and viscosity of ER fluid. Generally, the dielectric constant of silicone oil increases with rising temperature, which enhances the interfacial polarization of ER fluids.[50] Moreover, viscosities of ER fluids decrease with increasing temperature, which allows easy formations of fibril-like structure to enhance the ER activity.[51,52] Lastly, both ER activities measured by the cycling temperature test showed stable performances without fluctuation or instability up to 95.0 °C.

To further clarify the influence of ER fluid concentration and electric field strength, all of the ER fluids were evaluated as a function of volume fraction (Figure 8b) and applied electric field strength (Figure 8c). For the former, all of the samples were measured at a fixed shear rate (0.1 s^{-1}) and electric field strength (3.0 kV mm^{-1}) while increasing the volume fraction of spheres in 5.0% increments. ER efficiency increased with increasing volume fractions up to 30.0 vol %. Above 30 vol %, ER activity became unstable due to electrical shorts. Thus, all of the ER fluids exhibited the highest ER performance at 30.0 vol %. For the latter, all of the samples were dispersed in silicone oil (30.0 vol %) and the external electric field strength was carefully increased in increments of 0.5 kV mm^{-1}. Shear stress increased in proportion to a power of 1.5 up to 3.0 kV mm^{-1}. At higher field strengths, ER activity became unstable due to electrical shorts. On the basis of these data, optimal ER efficiency occurs at a volume fraction of 30.0 vol % and an electric field strength of 3.0 kV mm^{-1}.

The real-time reversibility of ER-fluids was examined by on−off switching tests under an electric field of 3.0 kV mm^{-1} (Figure 8d). Upon turning on the electric field, all of the ER fluids exhibited an immediate increase in shear stress. The Ca-HST-based ER fluids exhibited the highest shear stresses of ~62.3 Pa, which was 7.1-fold and 3.1-fold higher than those of the CS/ST and HST-based ER fluids, respectively. Upon turning off the electric field, all of the shear stresses returned immediately to their initial values. Interestingly, the ER performance of second switching was higher for all ER fluids because of the remaining preformed fibril-like structure from

DOI: 10.1021/acsami.5b02388
ACS Appl. Mater. Interfaces 2015, 7, 18977−18984

the first switching test. In other word, fibril-like structures formed on the first switching did not broke completely because of the low shear rate (0.1 s^{-1}) and short recovery time (10 s). Thus, ER fluids attained higher ER performance on the second switching test owing to the formation of more chain-like structures combined of first and second switching test. These data indicate excellent reversibility as a function of the presence of an external electric field.

Structural changes in all of the ER fluids were observed by optical microscopy (OM). Representative micrographs are shown in Figure 9. Well-dispersed ER fluids were placed between a pair of electrodes and the electric field was applied. Within a few tens of milliseconds, randomly distributed particles formed fibril-like structures along the direction of the electric field. This result demonstrates the versatile and rapid response of ER fluids composed of EM-HST spheres.

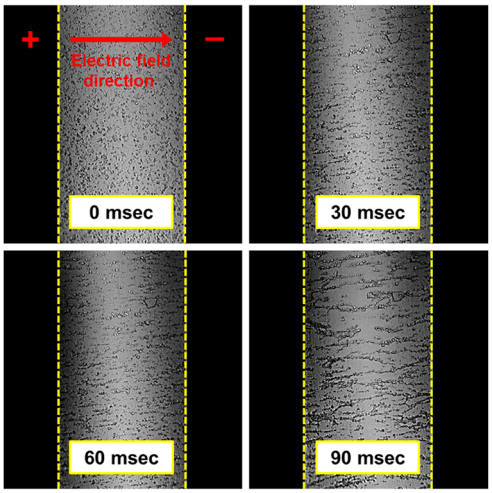

Figure 9. Optical microscope (OM) images of Ca-HST-based ER fluid under 3 kV mm^{-1} of external electric field. Randomly distributed ER fluid immediately formed fibril-like structure by applying an electric field. The gap between two electrodes was fixed to 1.0 mm.

CONCLUSION

In conclusion, various EM-HST spheres were successfully fabricated by sonication-mediated etching method using different $EM(OH)_2$ solutions. This simple approach effectively enhanced both dispersion stability and dielectric property in one-step process, while obtaining multigram scale of sample. The resulting EM-HST sphere-based ER fluids exhibited excellent ER activities relative to those of nonhollow CS/ST and undoped HST sphere-based ER fluids. Specifically, the Ca-HST-based ER fluids exhibited the highest shear stress of ca. 62.3 Pa, which was 7.1-fold and 3.1-fold higher than those of CS/ST and HST-based ER fluids, respectively. This drastic improvement in ER performance likely originates from enhanced particle mobility and the intrinsic interfacial polarization of EM-HST spheres. This study developed a simple means of enhancing the electro-response of materials by harnessing the synergetic effects of dispersibility and dielectric properties. Moreover, the applicability of our process to mass production will prove advantageous in commercial and practical applications.

ASSOCIATED CONTENT

Supporting Information

The Supporting Information is available free of charge on the ACS Publications website at DOI: 10.1021/acsami.5b02388.

(1) Core silica etching process with low and high concentrated etchants, (2) evolutionary mechanism of core/shell silica/titania to hollow silica/titania, (3) SEM micrographs of various EM-HST spheres, (4) BJH analysis of CS/ST, HST, and various EM-HST spheres, (5) BET analysis and pore volume calculation for CS/ST, HST, and various EM-HST spheres, (6) EDS elemental analysis of CS/ST, HST, and various EM-HST spheres, (7) XPS analysis of Ti 2p spectrum of various EM-HST spheres, (8) XPS analysis of specific Ca, Sr, and Ba metals, (9) physical parameters of various EM-HST spheres-based ER fluids, (10) ER activity of various EM-HST spheres-based ER fluids at zero field condition, and (11) cycling temperature test of various spheres-based ER fluids (PDF)

AUTHOR INFORMATION

Corresponding Author

*Tel.: 82-2-880-7069. Fax: 82-2-888-7295. E-mail: jsjang@plaza.snu.ac.kr.

Notes

The authors declare no competing financial interest.

REFERENCES

(1) Grzelczak, M.; Vermant, J.; Furst, E. M.; Liz-Marzán, L. M. Directed Self-Assembly of Nanoparticles. *ACS Nano* **2010**, *4*, 3591−3605.

(2) McIntyre, C.; Yang, H.; Green, P. F. Electrorheology of Suspensions Containing Interfacially Active Constituents. *ACS Appl. Mater. Interfaces* **2013**, *5*, 8925−8931.

(3) Hao, T. Electrorheological Fluids. *Adv. Mater.* **2001**, *13*, 1847−1857.

(4) Zhang, M.; Wang, L.; Wang, X.; Wu, J.; Li, J.; Gong, X.; Qin, J.; Li, W.; Wen, W. Microdroplet-Based Universal Logic Gates by Electrorheological Fluid. *Soft Matter* **2011**, *7*, 7493−7497.

(5) Kamelreiter, M.; Kemmetmüller, W.; Kugi, A. Digitally Controlled Electrorheological Valves and Their Application in Vehicle Dampers. *Mechatronics* **2012**, *22*, 629−638.

(6) Hong, J.-Y.; Jang, J. A Comparative Study on Electrorheological Properties of Various Silica−Conducting Polymer Core−Shell Nanospheres. *Soft Matter* **2010**, *6*, 4669−4671.

(7) Plachy, T.; Mrlik, M.; Kozakova, Z.; Suly, P.; Sedlacik, M.; Pavlinek, V.; Kuritka, I. The Electrorheological Behavior of Suspensions Based on Molten-Salt Synthesized Lithium Titanate Nanoparticles and Their Core-Shell Titanate/Urea Analogues. *ACS Appl. Mater. Interfaces* **2015**, *7*, 3725−3731.

(8) McIntyre, C.; Yang, H.; Green, P. F. Electrorheology of Polystyrene Filler/Polyhedral Silsesquioxane Suspensions. *ACS Appl. Mater. Interfaces* **2012**, *4*, 2148−2153.

(9) Plachy, T.; Sedlacik, M.; Pavlinek, V.; Trchová, M.; Morávková, Z.; Stejskal, J. Carbonization of Aniline Oligomers to Electrically Polarizable Particles and Their Use in Electrorheology. *Chem. Eng. J.* **2014**, *256*, 398−406.

(10) Plachy, T.; Sedlacik, M.; Pavlinek, V.; Morávková, Z.; Hajná, M.; Stejskal, J. An Effect of Carbonization on the Electrorheology of Poly(p-phenylenediamine). *Carbon* **2013**, *63*, 187−195.

(11) Hong, J.-Y.; Jang, J. Highly Stable, Concentrated Dispersions of Graphene Oxide Sheets and Their Electro-Responsive Characteristics. *Soft Matter* **2012**, *8*, 7348−7350.

DOI: 10.1021/acsami.5b02388
ACS Appl. Mater. Interfaces 2015, 7, 18977−18984

(12) Shin, K.-Y.; Lee, S.; Hong, S.; Jang, J. Graphene Size Control via a Mechanochemical Method and Electroresponsive Properties. *ACS Appl. Mater. Interfaces* **2014**, *6*, 5531−5537.
(13) Yoon, C.-M.; Lee, S.; Hong, S. H.; Jang, J. Fabrication of Density-Controlled Graphene Oxide-Coated Mesoporous Silica Spheres and Their Electrorheological Activity. *J. Colloid Interface Sci.* **2015**, *438*, 14−21.
(14) Lee, S.; Hong, J.-Y.; Jang, J. Synthesis and Electrical Response of Polyaniline/Poly(styrene sulfonate)-Coated Silica Spheres Prepared by Seed-Coating Method. *J. Colloid Interface Sci.* **2013**, *398*, 33−38.
(15) Liu, Y. D.; Quan, X.; Hwang, B.; Kwon, Y. K.; Choi, H. J. Core-Shell-Structured Monodisperse Copolymer/Silica Particle Suspension and Its Electrorheological Response. *Langmuir* **2014**, *30*, 1729−1734.
(16) Yin, J.; Chang, R.; Shui, Y.; Zhao, X. Preparation and Enhanced Electro-Responsive Characteristic of Reduced Graphene Oxide/Polypyrrole Composite Sheet Suspensions. *Soft Matter* **2013**, *9*, 7468−7478.
(17) Hao, T.; Kawai, A.; Ikazaki, F. Mechanism of the Electrorheological Effect: Evidence from the Conductive, Dielectric, and Surface Characteristics of Water-Free Electrorheological Fluids. *Langmuir* **1998**, *14*, 1256−1262.
(18) Kim, S. D.; Zhang, W. L.; Choi, H. J.; Seo, Y. P.; Seo, Y. Electrorheological Activity Generation by Graphene Oxide Coating on Low-Dielectric Silica Particles. *RSC Adv.* **2014**, *4*, 62644−62650.
(19) Kim, S.; Kim, C.; Hong, J.-Y.; Hwang, S. H.; Jang, J. Enhanced Electrorheological Performance of Barium-Doped SiO_2/TiO_2 Hollow Mesoporous Nanospheres. *RSC Adv.* **2014**, *4*, 6821−6824.
(20) Lee, J.; Hwang, S. H.; Yun, J.; Jang, J. Fabrication of SiO_2/TiO_2 Double-Shelled Hollow Nanospheres with Controllable Size via Sol−Gel Reaction and Sonication-Mediated Etching. *ACS Appl. Mater. Interfaces* **2014**, *6*, 15420−15426.
(21) Chen, Y.; Chu, C.; Zhou, Y.; Ru, Y.; Chen, H.; Chen, F.; He, Q.; Zhang, Y.; Zhang, L.; Shi, J. Reversible Pore-Structure Evolution in Hollow Silica Nanocapsules: Large Pores for siRNA Delivery and Nanoparticle Collecting. *Small* **2011**, *7*, 2935−2944.
(22) Hwang, S. H.; Yun, J.; Jang, J. Multi-Shell Porous TiO_2 Hollow Nanoparticles for Enhanced Light Harvesting in Dye-Sensitized Solar Cells. *Adv. Funct. Mater.* **2014**, *24*, 7619−7626.
(23) Chen, J.-F.; Wang, J.-X.; Liu, R.-J.; Shao, L.; Wen, L.-X. Synthesis of Porous Silica Structures with Hollow Interiors by Templating Nanosized Calcium Carbonate. *Inorg. Chem. Commun.* **2004**, *7*, 447−449.
(24) Choi, M.; Kim, C.; Jeon, S. O.; Yook, K. S.; Lee, J. Y.; Jang, J. Synthesis of Titania Embedded Silica Hollow Nanospheres *via* Sonication Mediated Etching and Re-Deposition. *Chem. Commun.* **2011**, *47*, 7092−7094.
(25) Baskaran, S.; Liu, J.; Domansky, K.; Kohler, N.; Li, X.; Coyle, C.; Fryxell, G. E.; Thevuthasan, S.; Williford, R. E. Low Dielctric Constant Mesoporous Silica Films Through Molecularly Templated Synthesis. *Adv. Mater.* **2000**, *12*, 291−294.
(26) Robertson, J. High Dielectric Constant Oxides. *Eur. Phys. J.: Appl. Phys.* **2004**, *28*, 265−291.
(27) Yin, J.; Xia, X.; Wang, X.; Zhao, X. The Electrorheological effect and Dielectric Properties of Suspensions Containing Polyaniline@Titania Nanocable-Like Particles. *Soft Matter* **2011**, *7*, 10978−10986.
(28) Yin, J.; Zhao, X. Titanate Nano-whisker Electrorheological Fluid With High Suspended Stability and ER Activity. *Nanotechnology* **2006**, *17*, 192−196.
(29) Shang, Y.; Ma, S.; Li, J.; Li, M.; Wang, J.; Zhang, S. Effect of Microstructure on Electrorheological Property for Pure TiO_2 Particle Material. *J. Mater. Sci. Technol.* **2006**, *22*, 572−576.
(30) Ma, S.-Z.; Liao, F.-H.; Li, S.-X.; Xu, M.-Y.; Li, J.-R.; Zhang, S.-H.; Chen, S.-M.; Huang, R.-L.; Gao, S. Effect of Microstructure, Grain Size, and Rare Earth Doping on the Electrorheological Performance of Nanosized Particle Materials. *J. Mater. Chem.* **2003**, *13*, 3096−3102.
(31) Wu, J.; Xu, G.; Cheng, Y.; Liu, F.; Guo, J.; Cui, P. The Influence of High Dielectric Constant Core on the Activity of Core−Shell Structure Electrorheological Fluid. *J. Colloid Interface Sci.* **2012**, *378*, 36−43.
(32) Oh, S. Y.; Oh, M. K.; Kang, T. J. Characterization and Electrorheological Response of Silica/Titania-Coated MWNTs Synthesized by Sol−Gel Process. *Colloids Surf., A* **2013**, *436*, 354−362.
(33) Zhang, H. B.; Edirisinghe, M. J.; Jayasinghe, S. N. Flow Behavious of Dielectric Liquids in an Electric Field. *J. Fluid Mech.* **2006**, *558*, 103−111.
(34) Kim, S.; Jang, Y.; Oh, W.-K.; Kim, C.; Jang, J. Fabrication of Barium- and Strontium-Doped Silica/Titania Hollow Nanoparticles and Their Synergetic Effects on Promoting Neuronal Differentiation by Activating ERK and p38 Pathways. *Adv. Healthcare Mater.* **2014**, *3*, 1097−1106.
(35) Wang, B. X.; Zhao, X. P. Wettability of Bionic Nanopapilla Particles and Their High Electrorheological Activity. *Adv. Funct. Mater.* **2005**, *15*, 1815−1820.
(36) Lee, B. M.; Kim, J. E.; Fang, F. F.; Choi, H. J.; Feller, J.-F. Rectangular-Shaped Polyaniline Tubes Covered with Nanorods and Their Electrorheology. *Macromol. Chem. Phys.* **2011**, *212*, 2300−2307.
(37) Hong, J.-Y.; Choi, M.; Kim, C.; Jang, J. Geometrical Study of Electrorheological Activity with Shape-Controlled Titania-Coated Silica Nanomaterials. *J. Colloid Interface Sci.* **2010**, *347*, 177−182.
(38) Huang, J. P.; Yu, K. W. AC Electrokinetics of the Microparticles in Electrorheological Solids. *Phys. Lett. A* **2004**, *333*, 347−353.
(39) Lee, S.; Yoon, C.-M.; Hong, J.-Y.; Jang, J. Enhanced Electrorheological Performance of a Graphene Oxide-Wrapped Silica Rods with a High Aspect Ratio. *J. Mater. Chem. C* **2014**, *2*, 6010−6016.
(40) Block, H.; Kelly, J. P.; Qin, A.; Watson, T. Materials and Mechanisms in Electrorheology. *Langmuir* **1990**, *6*, 6−14.
(41) Kim, S. D.; Zhang, W. L.; Choi, H. J. Pickering Emulsion-Fabricated Polystyrene−Graphene Oxide Microspheres and Their Electrorheology. *J. Mater. Chem. C* **2014**, *2*, 7541−7546.
(42) Chou, X.; Zhai, J.; Jiang, H.; Yao, X. Dielectric Properties and Relaxor Behavior of Rare-Earth (La, Sm, Eu, Dy, Y) Substituted Barium Zirconium Titanate Ceramics. *J. Appl. Phys.* **2007**, *102*, 084106.
(43) Raju, K. C. J.; Sivasubramanian, V.; Pragasam, R.; Viswanathan, B.; Murthy, V. R. K. Contributions to the Dielectric Constant of the System $BaLn_2Ti_4O_{12}$ from Packing Fraction and Nephelauxetic Ratio. *J. Appl. Phys.* **1993**, *74*, 1968−1971.
(44) Bhushan, B.; Basumallik, A.; Bandopadhyay, S. K.; Vasanthacharya, N. Y.; Das, D. Effect of Alkaline Earth Metal Doping on Thermal, Optical, Magnetic and Dielectric Properties of $BiFeO_3$ Nanoparticles. *J. Phys. D: Appl. Phys.* **2009**, *42*, 065004.
(45) Wang, B.; Zhao, X. Core/Shell Nanocomposite Based on the Local Polarization and Its Electrorheological Behavior. *Langmuir* **2005**, *21*, 6553−6559.
(46) Jiang, J.; Liu, Y. D.; Shan, L.; Zhang, X.; Meng, Y.; Choi, H. J.; Tian, Y. Shear Thinning and Shear Thickening Characteristics in Electrorheological Fluids. *Smart Mater. Struct.* **2014**, *23*, 015003.
(47) Cho, M. S.; Choi, H. J.; Jhon, M. S. Shear Stress Anlysis of a Semiconducting Polymer Based Electrorheological Fluid System. *Polymer* **2005**, *46*, 11484−11488.
(48) Lee, S.; Lee, J.; Hwang, S. H.; Yun, J.; Jang, J. Enhanced Electroresponsive Performance of Double−Shell SiO_2/TiO_2 Hollow Nanoparticles. *ACS Nano* **2015**, *9*, 4939−4949.
(49) Kim, S. G.; Lim, J. Y.; Sung, J. H.; Choi, H. J.; Seo, Y. Emulsion Polymerized Polyaniline Synthesized with Dodecylbenzene-Sulfonic Acid and Its Electrorheological Characteristics: Temperature Effect. *Polymer* **2007**, *48*, 6622−6631.
(50) Yin, J.; Zhao, X. Temperature Effect of Rare Earth-doped TiO_2 Electrorheological Fluids. *J. Phys. D: Appl. Phys.* **2001**, *34*, 2063−2067.
(51) Gonon, P.; Foulc, J.-N. Temperature Dependence of Particle−Particle Interactions In Electrorheological Fluids. *J. Appl. Phys.* **2000**, *87*, 3563.
(52) Yilmaz, H.; Degirmenci, M.; Unal, H.-I. Electrorheological Properties of PMMA-*b*-PSt Copolymer Suspensions. *J. Colloid Interface Sci.* **2006**, *293*, 489−495.

DOI: 10.1021/acsami.5b02388
ACS Appl. Mater. Interfaces 2015, 7, 18977−18984